

Detection of carbon monoxide trends in the presence of interannual variability

Sarah A. Strode^{1,2} and Steven Pawson²

Received 21 May 2013; revised 12 September 2013; accepted 18 October 2013; published 13 November 2013.

[1] Trends in fossil fuel emissions are a major driver of changes in atmospheric CO, but detection of trends in CO from anthropogenic sources is complicated by the presence of large interannual variability (IAV) in biomass burning. We use a multiyear model simulation of CO with year-specific biomass burning to predict the number of years needed to detect the impact of changes in Asian anthropogenic emissions on downwind regions. Our study includes two cases for changing anthropogenic emissions: a stepwise change of 15% and a linear trend of 3% yr⁻¹. We first examine how well the model reproduces the observed IAV of CO over the North Pacific, since this variability impacts the time needed to detect significant anthropogenic trends. The modeled IAV over the North Pacific correlates well with that seen from the Measurements of Pollution in the Troposphere (MOPITT) instrument but underestimates the magnitude of the variability. The model predicts that a 3% yr⁻¹ trend in Asian anthropogenic emissions would lead to a statistically significant trend in CO surface concentration in the western United States within 12 years, and accounting for Siberian boreal biomass-burning emissions greatly reduces the number of years needed for trend detection. Combining the modeled trend with the observed MOPITT variability at 500 hPa, we estimate that the 3% yr⁻¹ trend could be detectable in satellite observations over Asia in approximately a decade. Our predicted timescales for trend detection highlight the importance of long-term measurements of CO from satellites.

Citation: Strode, S. A., and S. Pawson (2013), Detection of carbon monoxide trends in the presence of interannual variability, *J. Geophys. Res. Atmos.*, 118, 12,257–12,273, doi:10.1002/2013JD020258.

1. Introduction

[2] Detection of long-term trends in carbon monoxide (CO) both within and downwind of source regions is important as CO is the main sink of the hydroxyl radical (OH), the primary atmospheric oxidant, and an ozone precursor [Crutzen, 1973; Logan *et al.*, 1981; Thompson, 1992]. Both anthropogenic sources and biomass burning are major contributors to CO emissions, and separating their effects is essential for attributing CO trends. Lamarque *et al.* [2010] estimate that global anthropogenic CO emissions increased from 584 Tg in 1980 to 627 Tg in 1990, a 7% increase, and then decreased by 3% to 608 Tg in 2000. Van der Werf *et al.* [2006] estimated global biomass burning emissions of CO to average 433 Tg yr⁻¹ over the 1997–2004 period, but emissions for 1998 were 591 Tg, 36% higher than the mean. Regionally, such interannual anomalies in biomass-burning sources can obscure the signal from more slowly changing anthropogenic emissions.

[3] There is also considerable uncertainty in CO emissions for a given year. A comparison of emission inventories [Graniér *et al.*, 2011] shows differences of up to 9% for global anthropogenic CO emissions and 19% for global biomass-burning CO for 2005, with larger differences in some regions. An inversion study by Kopacz *et al.* [2010] suggested that total CO emissions are much higher than bottom-up inventories suggest. Variability in atmospheric transport [Allen *et al.*, 1996] and oxidant concentrations [Duncan and Logan, 2008] also contribute to CO variability. Consequently, controlled model studies can be useful for determining signal levels expected on the basis of known inputs and to help optimize observing systems for signal detection by identifying time frames and key regions for trend detection.

[4] The strength and the direction of the anthropogenic trend vary by region; further complicating trend detection since CO's lifetime of 1–2 months [Bey *et al.*, 2001] allows it to impact regions distant from its sources. The introduction of regulations to limit pollution led to CO emissions from the United States decreasing by an estimated 38% between 1990 and 2006 [U.S. Environmental Protection Agency, 2008]. In contrast, Asian emissions increased from 207 Tg in 1980 to 277 Tg in 1990 and 305 Tg in 2000, a 47% increase in 20 years [Ohara *et al.*, 2007]. Four representative concentration pathways [Van Vuuren *et al.*, 2011] used in future climate scenarios include differences in both the sign and strength of the projected trend in Asian CO emissions between scenarios for 2020–2040. Given the importance and uncertainty in

¹Universities Space Research Association, Columbia, Maryland, USA.

²NASA Goddard Space Flight Center, Greenbelt, Maryland, USA.

Corresponding author: S. A. Strode, NASA Goddard Space Flight Center, 8800 Greenbelt Rd., Code 614, Greenbelt, MD 20771, USA. (Sarah.a.strode@nasa.gov)

future Asian anthropogenic emission trends, it is useful to identify regions where observations will be able to detect these changes.

[5] Surface observations show global CO concentrations increasing in the early 1980s and then decreasing from 1987–1992 [Khalil and Rasmussen, 1988; Khalil and Rasmussen, 1994]. Novelli *et al.* [2003] found a decrease in Northern Hemisphere CO concentrations measured at the NOAA Climate Monitoring and Diagnostics Laboratory sites from 1991–2001, likely attributable to decreases in emissions. A modeling study by Duncan and Logan [2008] shows a negative trend in high northern latitude CO for 1988–1997, with a strong impact from decreasing fossil fuel emissions from Europe. Satellite observations from nadir-viewing thermal infrared (TIR) instruments show decreasing trends in the CO column for China, the eastern United States, and Europe [Worden *et al.*, 2013].

[6] Observations also show strong interannual variability (IAV) in global CO concentrations due to the variability in biomass burning [Langenfelds *et al.*, 2002; Novelli *et al.*, 2003]. Enhanced CO from biomass burning during El Niño years is evident in satellite observations from the Measurements of Pollution in the Troposphere (MOPITT) instrument [Edwards *et al.*, 2006; Yurganov *et al.*, 2008], Atmospheric Infrared Sounder (AIRS) [McMillan *et al.*, 2008], and the Tropospheric Emission Spectrometer (TES) instrument [Logan *et al.*, 2008]. Szopa *et al.* [2007] examined surface station CO for the 1997–2001 period. They attribute most of the tropical variability to meteorological variability, while for the high latitudes, they find that biomass burning and meteorological variability make nearly equal contributions. Voulgarakis *et al.* [2010] found that variability in emissions explained much of the CO IAV in both Europe and Indonesia.

[7] On a regional scale, both biomass burning and long-range transport contribute to CO IAV over the North Pacific and western North America. Jaffe *et al.* [2004] found that the areal extent of Russian biomass burning has a statistically significant correlation with CO concentrations at sites in the western United States. An analysis of 2000–2006 by Pfister *et al.* [2010] found that emissions and transport contribute approximately equally to the IAV of CO loading over the Pacific, while meteorology explained two thirds of the IAV over the U.S. Liang *et al.* [2005] showed that an index based on North Pacific sea level pressure anomalies could explain over half the interannual variance in trans-Pacific transport of CO. The outflow of CO from Asia also has a strong seasonal cycle, with the peak outflow occurring in March and the minimum in summer [Liu *et al.*, 2003].

[8] The purpose of this study is to identify regions and timescales for detecting changes in anthropogenic CO emissions. Our primary focus is on the influence of changes in Asian emissions on trends over the Pacific, as this region is subject to influences from both changing anthropogenic emissions from a major source region and IAV in both biomass burning and long-range transport. We conduct a multiyear model simulation using variable biomass-burning emissions and meteorology from an atmospheric reanalysis to estimate the level of CO IAV that an observing system would encounter in various regions of the atmosphere. We then vary the model's CO contribution from Asian anthropogenic sources and examine when and where these anthropogenic changes can be separated from the background variability.

Section 2 describes the model setup. Section 3 includes a comparison of the model's IAV to the IAV observed by surface and satellite observations and a discussion of the factors contributing to this variability. Our methodology for examining trends is described in section 4. In section 5, we compare the magnitude of the IAV to the response to changes in anthropogenic emissions. Based on the variability, we estimate the number of years needed to detect a trend in anthropogenic emissions. In section 6, we present conclusions and discuss the implications for observing trends from ground or space-based measurements.

2. Carbon Monoxide Simulations with GEOS-5

[9] The simulations examined in this work use the Goddard Earth Observing System, version 5 (GEOS-5) atmospheric general circulation model constrained by meteorological analyses. This approach ensures that the simulations follow a realistic trajectory with year-to-year variations in meteorology that are consistent with the specified CO emissions from biomass burning. The simulations cover the period from 2000–2011 and are constrained by the meteorological analyses from the Modern-Era Retrospective analysis for Research and Applications system [Rienecker *et al.*, 2011].

[10] GEOS-5 uses the finite-volume dynamical core with a quasi-Lagrangian vertical coordinate [Lin, 2004], along with a comprehensive package of physical parameterizations [Rienecker *et al.*, 2008]. The simulations in this work have a horizontal resolution of $2^\circ \times 2.5^\circ$ and 72 layers. Following Ott *et al.* [2010], we use a simple representation of CO with atmospheric loss that is proportional to a prescribed, three-dimensional monthly OH field. Multiple “tagged CO” tracers are included, in order to attribute the contributions of CO from different regions and source types to the total CO sampled at any location. The tagged tracers include CO from Asian anthropogenic (AA) sources, North American anthropogenic sources, biomass burning over Russia, global biomass burning (BB), and oxidation of methane and other hydrocarbons, as well as emissions from several other regions. The three-dimensional methane concentration and CO sources from oxidation of biogenic hydrocarbons are also prescribed as monthly means. Anthropogenic and biomass-burning CO emissions are amplified by scaling factors to account for the oxidation of co-emitted nonmethane hydrocarbons. The linearization of the chemical loss means that it can be applied individually to each of the tagged CO tracers. Scaling up or down a particular tagged tracer provides a computationally efficient method of estimating the impact of increasing or decreasing the strength of any emission source, and we apply this method to estimate the impact of a change in Asian anthropogenic emissions in section 5.

[11] Monthly and interannually varying biomass-burning emissions for our standard simulation are from the Global Fire Emissions Database, version 3 (GFED3) [Van der Werf *et al.*, 2010] for our standard simulation. We also conduct sensitivity studies, discussed in section 3, using monthly emissions from the Global Fire Emissions Database, version 2 (GFEDv2) [Van der Werf *et al.*, 2006] and GFED3 with daily variability [Mu *et al.*, 2011]. All biomass-burning emissions are injected in the boundary layer. The baseline anthropogenic emissions are the 2005 values from the Coupled Model Intercomparison Project Phase 5 [Lamarque *et al.*, 2010].

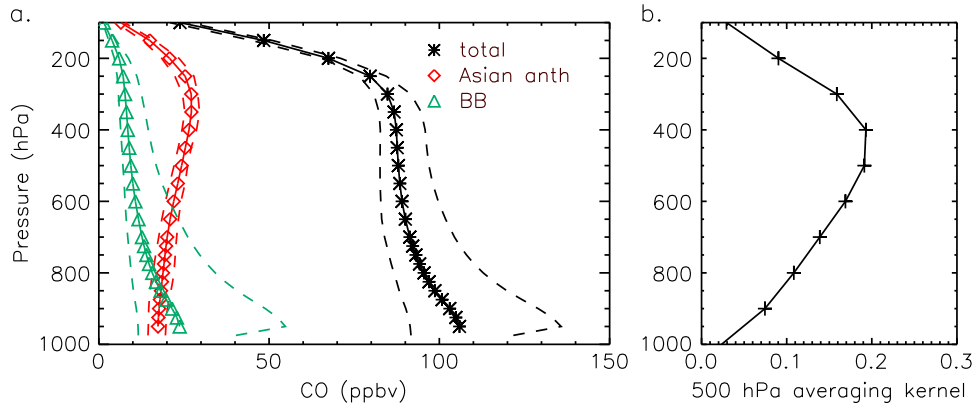


Figure 1. (a) 2000–2011 multiyear mean September profiles of total model CO (black stars), tagged Asian anthropogenic CO (red diamonds), and tagged biomass-burning CO (green triangles) over the northeast Pacific (178°W – 130°W , 30° – 55°N) are shown with solid lines and symbols. The maximum and minimum values for each tracer from the September means are shown in dashed lines. (b) The mean September MOPITT 500 hPa level averaging kernel for the same region and time period.

3. Comparison to Observations

[12] The length of the data record needed to detect trends due to Asian anthropogenic emissions depends on the magnitude of the change compared to the strength and variability of other emission sources. The drivers of CO trends and variability depend both on distance from source regions and the altitude considered, so satellite and surface observations can provide complementary data on trends and variability. Figure 1a compares the average vertical profiles for September (2000–2011) of the simulated total CO, AA CO, and BB CO over the northeast Pacific. We focus on this region because of its location downwind of Asian anthropogenic sources. Together, the AA and BB sources contribute about 40% to the mean total CO in this region at all altitudes. CO from methane oxidation (not shown) is another major contributor, but its variability is relatively small [Duncan *et al.*, 2007]. The IAV of the AA CO, which depends on IAV in transport across the Pacific, is quite small at all levels. In contrast, large IAV is present in the BB CO, which is driven by the Russian BB tracer in September. Previous studies have shown that IAV in boreal biomass burning is correlated with high Northern Hemisphere summer CO IAV [Wotawa *et al.*, 2001; Kasischke *et al.*, 2005]. Our tagged tracers show a range of BB CO concentrations from about 10 to 50 ppbv, with a mean near 20 ppbv, near the surface. The IAV in BB CO remains quite large throughout the troposphere, and it is the dominant contribution to the IAV of the total CO at all levels (Figure 1a).

[13] The warm conveyor belts of midlatitude cyclones can lift anthropogenic CO from Asia into the free troposphere [e.g. Stohl, 2001], and this mechanism is important for transpacific transport in autumn [Hsu *et al.*, 2012; Liang *et al.*, 2004]. Liang *et al.* [2004] showed enhanced Asian anthropogenic CO in the upper troposphere compared to the lower during September above Cheeka Peak, Washington. Figure 1a shows that the biomass-burning tracer concentration exceeds that of the Asian anthropogenic tracer at the surface over the northeast Pacific, while the Asian anthropogenic tracer increases with altitude and dominates in the middle and upper troposphere. This shift in the relative contributions

of AA and BB CO with altitude is consistent with the findings of Pfister *et al.* [2011a, 2011b] for the eastern Pacific during the Arctic Research of the Composition of the Troposphere from Aircraft and Satellites campaign.

[14] The vertical distribution of CO from different sources is important for trend detection from satellites since the sensitivity of nadir-viewing TIR satellite instruments varies with altitude. For example, the vertical sensitivity of the TIR retrievals of the Measurements of Pollution in the Troposphere (MOPITT) instrument on NASA’s EOS Terra satellite is greatest between 700 and 500 hPa, and the CO column averaging kernel has a maximum around 500 hPa [Emmons *et al.*, 2007]. Figure 1 shows that the AA CO is the dominant contributor at the level where the MOPITT 500 hPa kernel is most sensitive (Figure 1b). The large IAV of the biomass-burning tracer (dashed green lines), which drives much of the total CO IAV (dashed black lines), also decreases with altitude. Consequently, we examine the role of CO variability both at the surface, where emissions originate, and in the midtroposphere, where future trends may be detectable in space-based observations.

[15] The variability of modeled CO concentrations is compared to observations from surface sites and satellites, focusing on the North Pacific. The NOAA Global Monitoring Division (GMD) observation network [Novelli and Masarie, 2010] provides over 20 years of data on CO concentrations at surface sites. Our analysis uses the monthly mean GMD CO product, which is created by sampling from a smooth curve [Thoning *et al.*, 1989], as well as the discreet weekly data.

[16] CO measurements are also available for several satellite-based instruments, providing the potential to detect trends over many geographic regions. Nadir-viewing TIR instruments provide valuable constraints on trends and variability in the CO column [Worden *et al.*, 2013]. The sensitivity of these instruments to midtropospheric CO [e.g., Deeter *et al.*, 2004; George *et al.*, 2009] complements the constraints on surface CO provided by the GMD data. CO columns from TIR instruments are available from MOPITT, AIRS on the EOS Aqua satellite [Aumann *et al.*, 2003; McMillan *et al.*, 2005], TES on the Aura satellite

STRODE AND PAWSON: DETECTION OF CO TRENDS VERSUS IAV

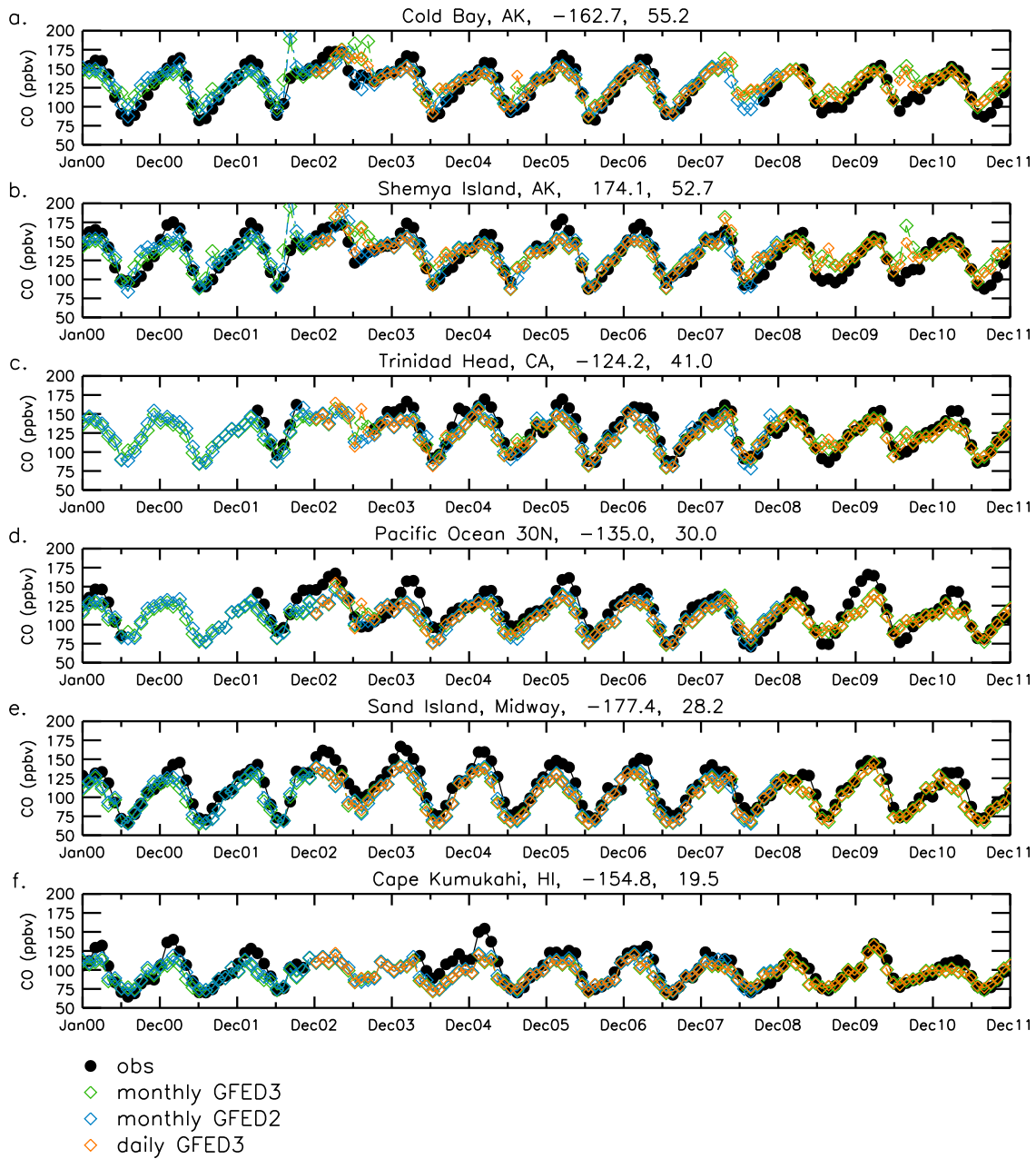


Figure 2. Twelve year time series of the NOAA Global Monitoring Division (GMD) CO observations (black circles) from six sites in the North Pacific region, overplotted with modeled CO. The standard model simulation (green diamonds) used monthly biomass burning from the GFED3 inventory. Sensitivity simulations using monthly biomass burning from the GFED2 inventory (blue diamonds) and daily biomass burning emissions from GFED3 (orange diamonds) are also shown. From top to bottom, the six sites are the following: Cold Bay, AK (CBA: 162.7°W, 55.2°N); Shemya Island, AK (SHM: 174.1°E, 52.7°N); Trinidad Head, CA (THD: 124.2°W, 41.0°N); Pacific Ocean, 30°N (POCN30: 135°W, 30°N); Sand Island, Midway (MID: 177.4°W, 28.2°N); and Cape Kumukahi, HI (KUM: 154.8°W, 19.5°N).

[Rinsland *et al.*, 2006], and the Infrared Atmospheric Sounding Interferometer (IASI) on the MetOp satellite [Clerbaux *et al.*, 2009]. The MOPITT instrument, operating since March 2000, provides near-global coverage of CO concentrations [Edwards *et al.*, 2004] in three days. We focus on MOPITT in this study because it provides the longest observation record.

[17] MOPITT CO has been validated against in situ and aircraft observations [Emmons *et al.*, 2004, 2007, 2009;

Deeter *et al.*, 2010]. We use CO column and 500 mb daytime data from the MOPITT version 4 [Deeter *et al.*, 2010] level 3 daily gridded product. The version 4 product exhibits a bias of less than a percent and a drift of approximately 1 ppbv yr⁻¹ at the 700 hPa level, while the 400 hPa level exhibits a negative bias of 6% and a drift of approximately 2 ppbv yr⁻¹ [Deeter *et al.*, 2010]. In 2001, the instrument configuration changed due to a cooler failure [Emmons *et al.*, 2004]. MOPITT v4 uses a monthly climatology from the Model for Ozone and

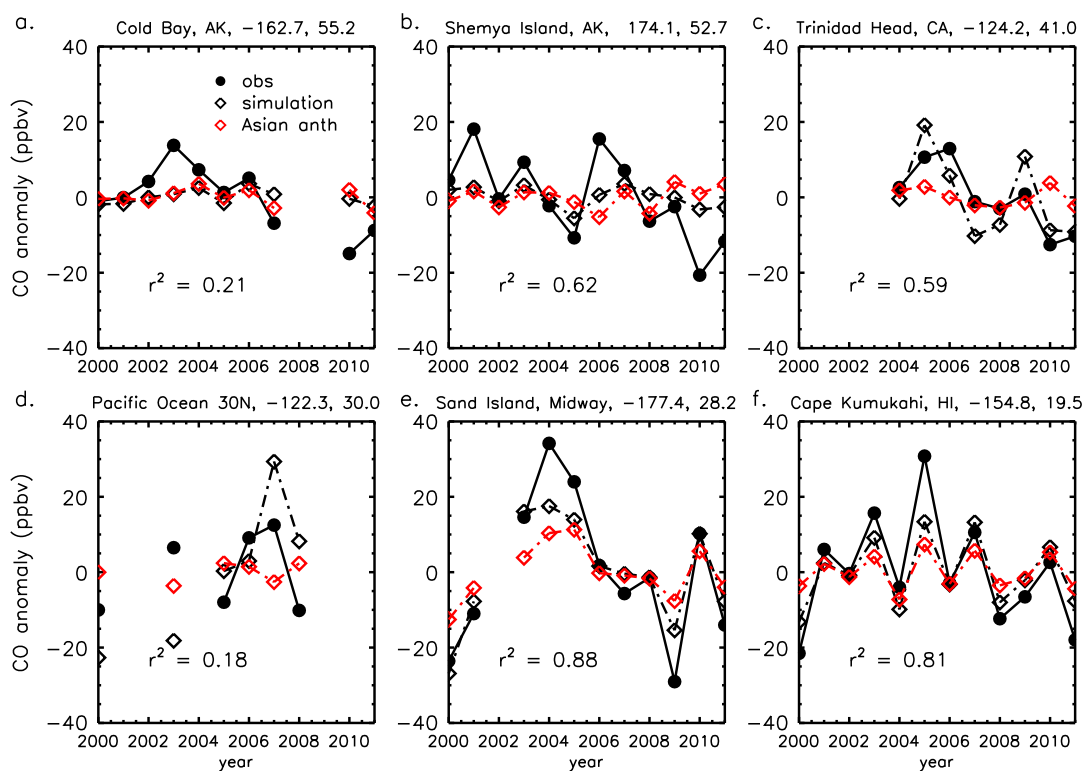


Figure 3. Yearly anomalies of observed (black circles) and simulated (open diamonds) February CO concentrations at GMD sites. Anomalies in the model’s Asian anthropogenic CO tracer are shown in red. Comparisons are for the same six sites shown in Figure 2: (a) Cold Bay, Alaska; (b) Shemya Island, Alaska; (c) Trinidad Head, California; (d) Pacific Ocean, 30°N; (e) Sand Island, Midway; and (f) Cape Kumukahi, Hawaii.

Related chemical Tracers 4 model for its a priori CO profiles [Deeter *et al.*, 2010]. The degrees of freedom for signal vary by location, with higher values over land and in the tropics [Deeter *et al.*, 2004], reaching up to approximately 1.5 in the zonal mean for MOPITT version 4 [Deeter *et al.*, 2010]. We also use the AIRS version 5 [McMillan *et al.*, 2011] monthly gridded column CO product, since AIRS provides additional global data on CO beginning in 2002. Its sensitivity is greatest between 600 and 300 hPa, and the treatment of cloudy pixels increases its horizontal coverage compared to MOPITT [Warner *et al.*, 2007].

[18] Figure 2 compares monthly mean modeled CO with the monthly observations from six GMD surface sites in the North Pacific region. For comparison to the Trinidad Head data, the model was sampled one grid box to the west in order to sample marine inflow. However, Trinidad Head receives a mixture of background and polluted air, which may lead to some of the mismatches between the model and observations at this site. The figure includes sensitivity simulations using monthly GFED2 and daily GFED3 BB emissions, as well as the standard simulation using monthly GFED3 BB emissions. While sensitivity to the choice of BB emissions is evident at some times, such as the summer of 2003, the three options yield similar results over most of the time series, justifying the use of the monthly GFED3 BB values for our analysis. The model simulation gives a reasonable reproduction of the mean and seasonal cycle observed at these GMD sites, but it does underestimate many of the seasonal peak values seen in the observations.

[19] The analysis focuses on two months, February and September, which have weak and strong boreal BB influence in the North Pacific, respectively. Since CO shows substantial weekly as well as interannual variability, for this analysis, we use the discreet GMD data, which has a sampling frequency of approximately once per week at land sites [Novelli and Masarie, 2010]. We construct monthly means of the discreet GMD data by filtering out any data with a rejection or selection flag, averaging the remaining observations within each day, and then averaging all February or September days for the given year. We then sample the model at the GMD locations and construct new model monthly means at these locations by averaging the model output for only the days with a corresponding observation. This method gives model means consistent with the sampling frequency of the GMD observations. Removing the 12 year mean of the given month yields the annual monthly CO anomalies.

[20] The IAV of surface CO at the six GMD sites in the North Pacific region in February is shown in Figure 3. The modeled anomalies at Midway (Figure 3e) and Cape Kumukahi (Figure 3f) are highly correlated with the observed anomalies ($r^2=0.88$ and 0.81 , respectively), and the tagged tracers show that variability in the Asian anthropogenic tracer drives much of the IAV at this location. Jaffe *et al.* [1997] found that most of the high CO events at Midway Island and Mauna Loa, Hawaii are associated with springtime transport from Asia. Midway and Cape Kumukahi also have the largest amplitude in the anomalies.

Table 1. Correlation and Bias of the Modeled IAV Versus GMD and MOPITT Observations^a

Comparison	Correlation (r^2)	Mean Bias (%)	% Bias in Standard Deviation
Feb GMD	0.55 (0.18–0.88)	-7 (-3 to -11)	-19 (-76 to 80)
Sept GMD	0.61 (0.19–0.89)	9 (-4 to 25)	16 (-54 to 75)
Feb MOPITT	0.69	-12	-38
April MOPITT	0.46	-18	-26
Sept MOPITT	0.58	-5	-18

^aThe values given for the GMD comparison are the mean for the six sites, while the values in parentheses show the range across the six sites.

The strong correlation suggests that the model reproduces important transport processes that contribute to IAV at these sites.

[21] The modeled IAV has much lower correlation with the observations at Cold Bay and the Pacific Ocean 30°N. It captures over half of the variance at Shemya Island and Trinidad Head, but the magnitude of the model IAV at Shemya Island is smaller than the observed (Figure 3). We do not expect the model to capture all of the variability seen in the observations given the fairly coarse resolution and simplified nature of the CO simulation, which neglects variability in OH concentrations and non-BB emissions. Considering all six sites, the model has a correlation of .55 with the deseasonalized data but underestimates the standard deviation in February by 19% (Table 1). An underestimate of the standard deviation will contribute to an underestimate of how much data is needed to achieve statistical significance.

[22] The CO variations in September (Figure 4) at the same six stations show large positive anomalies in 2002 and 2003 in both the model and observations. In the summer of 2003, strong biomass burning in Russia led to enhanced CO

concentrations [Edwards et al., 2004]. MacDonald et al. [2011] observed anomalously high CO at Whistler Peak in Western Canada during September–October 2002 and April–August 2003, consistent with the timings of high Siberian biomass burning. Increased concentrations in ship-based observations during 2002/2003 also related to the large Siberian fires [Yashiro et al., 2009]. Our tagged tracers confirm that Russian biomass burning is the main driver of the large CO anomalies in September for this period at the Alaskan sites (Figure 4). There is a strong correlation between the modeled and observed anomalies (Table 1 and Figure 4) for September, but the model overestimates the 2002 anomaly at the Alaskan sites (Figures 4a and 4b). The mean bias in the model is less than 10% in both February and September. The model standard deviation is biased high compared to the observations in September (Table 1).

[23] Transport in the free troposphere is an important contributor to the influence and variability of Asian CO over the Pacific and North America [Bey et al., 2001; Liu et al., 2003; Stohl et al., 2002; Yienger et al., 2000], and the transport of CO across the Pacific is seen in MOPITT observations [Allen et al., 2004; Heald et al., 2003; Turquety et al., 2008].

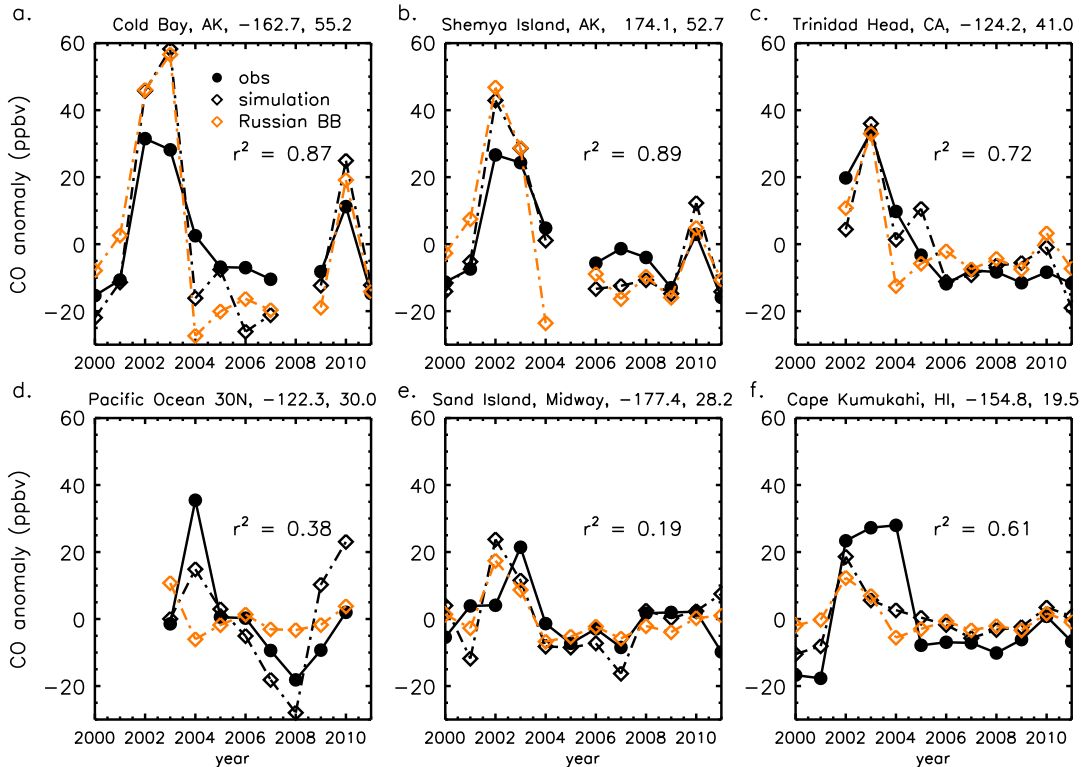


Figure 4. As in Figure 3 but for September. The additional orange line represents anomalies in the model tracer of Russian biomass-burning CO.

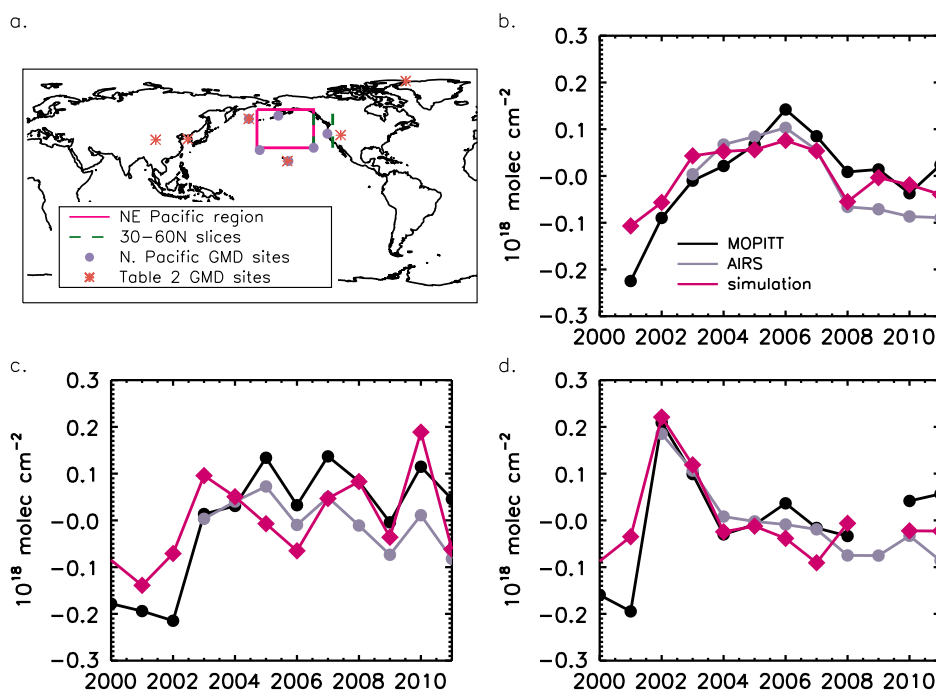


Figure 5. (a) Map of the regions discussed in this study including the GMD sites in Figures 2–4 (gray circles) and Table 2 (red stars), slices discussed in Figure 6 (dashed green lines), and (b–d) the MOPITT region used (magenta box). Figure 5b shows the annual February anomaly in the CO column for the region bounded by 30°N – 60°N , 179.5°W – 135°W from MOPITT (black line) and AIRS (gray line). The model simulation (magenta line) is convolved with the MOPITT averaging kernel and a priori for comparison to MOPITT. The same quantities are shown for April in Figure 5c and September in Figure 5d.

Consequently, we next examine the model’s ability to reproduce midtropospheric inflow into the U.S. by comparing the model’s CO column anomalies to MOPITT anomalies for a slice from 30°N – 60°N , 179.5°W – 135°W . This region is shown by the magenta box in Figure 5a, along with the locations of the GMD sites (gray circles) discussed above. We use the daily MOPITT averaging kernels to convolve the daily model profiles with the MOPITT a priori information for each day within the month and then average over the month.

[24] The model anomalies compared to MOPITT for February, April, and September are shown in Figures 5b–5d, respectively. We include April in this figure because it is a month with both biomass burning influence and strong transport from Asia to the Pacific. The anomaly in AIRS CO is also plotted for qualitative comparison, noting that the AIRS vertical sensitivity is different from that of MOPITT. The model IAV has a strong correlation with that of MOPITT: r^2 values are 0.69, 0.46, and 0.58 for February, April, and September, respectively (Table 1). These correlations are statistically significant at the 95% level based on the two-tailed student’s t test. The model does not capture all the year-to-year variations seen in the MOPITT data, but some of the observed anomalies are only a few percent, within the uncertainty of the MOPITT CO column. The model’s standard deviation is smaller than that of the observations, especially in February (Table 1), and the model mean is biased low. A low bias compared to MOPITT in the northern midlatitudes is a common feature seen in multimodel studies [Shindell *et al.*, 2006; Naik *et al.*, 2013]. The tagged tracers

show that the model’s September IAV is dominated by a large increase in Russian biomass burning in 2002, while variability in the Asian anthropogenic contribution is important in February.

[25] In summary, the model is able to simulate some of the large enhancements in CO due to anomalously high biomass burning. It also correlates well with the IAV in the CO column in February, a month in which Asian anthropogenic CO makes a larger contribution. The simulation underestimates the variability at surface sites in February and in the column CO observed by MOPITT in February, April, and September. A possible cause of the model underestimate of the variability, especially in September, is the injection of all BB emissions into the model boundary layer. In reality, some BB emissions occur above the boundary layer [Val Martin *et al.*, 2010], altering their subsequent transport. Another factor could be the use of a fixed OH field. Duncan and Logan [2008] found that OH varied by $\pm 10\%$ for the period from 1988–1997. Our simulation’s underestimate of variability means that the model-based estimates of time needed for trend detection, presented in the next section, are likely lower bounds. However, the model’s ability to capture key features in the observed IAV suggests that it is a useful tool for identifying optimal regions for trend detection.

4. Methods

[26] Given the computational expense of running multiyear chemistry simulations, it is useful to predict the number of years needed ahead of time. Furthermore, to the extent that

the model reproduces the observed variability, multiyear simulations of different emission scenarios provide a basis for estimating how many years of observations in different regions are needed to detect a change in emissions.

[27] We quantify the impacts of $\pm 15\%$ or $\pm 30\%$ changes in AA emissions by scaling the AA “tagged” tracer. This allows us to test our ability to detect emission changes of different magnitudes using simulations with realistically varying biomass burning. We then use our model simulation to estimate how many years of measurements would be necessary to detect a statistically significant change in the decadal mean due to a 15% decrease in Asian anthropogenic emissions. *Taschetto and England* [2008] found that for variables with unknown distributions, the necessary ensemble size is approximately 15% larger than would be calculated with a normal distribution. In this study, we make the simplifying assumption of a normal distribution for CO concentration in order to use the student’s t test to determine significance.

[28] We define the change as detectable at a given grid box if the mean of the -15% case has a statistically significant difference from the standard simulation at the 5% significance level, based on a one-tailed t test. The test statistic for the difference of means is given by

$$t = \frac{X_2 - X_1}{s_p \sqrt{\frac{1}{N_1} + \frac{1}{N_2}}} \quad (1)$$

where X_1 and X_2 are the sample means of the standard and reduced emission cases, $N_1 = N_2 = N$ is the number of years of each emission case, and s_p is the pooled estimate of their common standard deviation [e.g., *von Storch and Zwiers*, 1999]. We apply this test iteratively to a given month (either February or September), so that there is one sample per year, and increase N until we are able to reject the null hypothesis using the s_p and $X_2 - X_1$ calculated from our 12 year sample. Since the lifetime of CO is much shorter than 1 year, we assume the values for each year are independent of each other.

[29] We also use the model to estimate the years needed to detect a linear trend in Asian anthropogenic emissions by increasing the AA tagged tracer by $3\% \text{ yr}^{-1}$. The magnitude of the trend relative to the unexplained variability and autocorrelation of the noise in the data together determine whether a statistically significant trend is detectable [*Weatherhead et al.*, 2002]. Autocorrelation is important for our simulated CO trends because we are using the monthly averages of the modeled CO for each month, but the lifetime of CO is long enough that we cannot assume each month is independent of the previous month. *Tiao et al.* [1990] and *Weatherhead et al.* [1998] showed that the number of years of data needed to detect a trend with a probability of 0.9 at the 95% confidence level is approximated by

$$n^* \approx \left(\frac{3.3\sigma_N}{|\omega_0|} \sqrt{\frac{1+\varphi}{1-\varphi}} \right)^{2/3} \quad (2)$$

where n^* is the required number of years, ω_0 is the trend per year, σ_N is the standard deviation of the noise, and φ is the autocorrelation of the noise between one monthly measurement and the next, assuming the noise is autoregressive order 1 noise and $|\varphi| < 1$. Here we apply this method to our modeled CO trend and variability.

[30] We decompose our simulated CO time series of monthly mean data at each grid box into a constant (μ), trend (ω), seasonal cycle (S), and noise (N):

$$C(t) = \mu + S(t) + \omega^*(t/12) + N(t) \quad (3)$$

where t is in months using multiple regression analysis to determine the best fit to μ , ω , and S . We then calculate the standard deviation and autocorrelation of the noise (N) in each grid box and apply equation (2) to estimate the number of years (n^*) needed to detect a significant trend.

[31] Previous studies have shown that burned area in boreal Russia can explain approximately one third to one half of the summertime interannual variations in extratropical Northern Hemisphere CO [*Kasischke et al.*, 2005; *Wotawa et al.*, 2001]. Consequently, we conduct a sensitivity study adding the monthly anomalies in the biomass-burning CO emissions from GFED3 for the region of Asiatic Russia as a predictor in equation (3) to obtain the following equation:

$$C(t) = \mu + S(t) + \omega^*(t/12) + B(t) + N(t) \quad (4)$$

where B is the monthly anomalies in GFED3 CO emissions from Asiatic Russia. We then recalculate the trend and noise terms using equation (4). Since we used GFED3 CO emissions in our simulation, this predictor assumes we have perfect knowledge of biomass-burning emissions on a regional scale but does not assume that we have perfect knowledge of its transport to each grid box.

5. Trend Detection

5.1. Surface Response to a Stepwise Emission Change

[32] The results of section 3 demonstrate the model’s ability to capture a substantial portion of the IAV seen in both satellite and ground-based observations, particularly the variability due to biomass burning. In this section, we use the methods described in section 4 to examine when and where hypothetical stepwise changes in Asian anthropogenic emissions are distinguishable from atmospheric variability in surface CO.

[33] Figure 6a shows the February IAV of modeled CO averaged over 30°N – 60°N at the surface at 135°W , upwind of North America. Imposing increases or decreases in the Asian anthropogenic emission tracer leads to a new mean and IAV of total CO. There is overlap in the error bars between the 0 and 15% changes in Asian anthropogenic emissions, but the standard deviations for the 0 and 30% cases do not overlap. Consequently, a change of 30% or more in Asian emissions should be detectable using surface observations in this region and season. Since most surface measurements are made on land, we consider another February slice located at 120°W , in the western United States. The dashed green lines in Figure 5a shows the location of the two slices. The surface variability in this region (Figure 6b) leads to overlap in the error bars between the different emission scenarios. However, if we assume the North American anthropogenic contribution is perfectly known, we can subtract the North American anthropogenic CO from the total tracer. This leads to a CO signal with small IAV, as shown by the blue error bars, and the Asian emission scenarios are distinguishable.

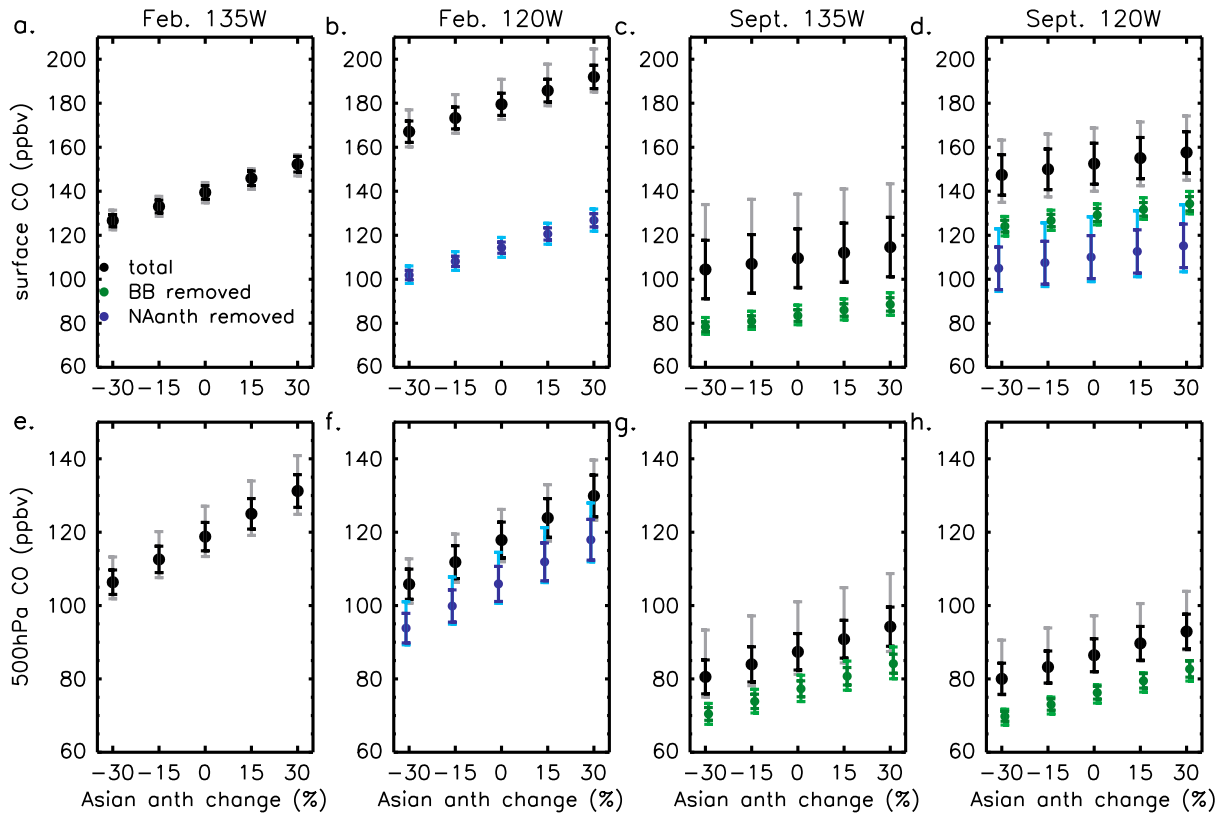


Figure 6. Mean and interannual variability of February model CO at the surface for (a) 30°N – 60°N , 135°W and for (b) 30°N – 60°N , 120°W for changes of -30% , -15% , 0% , $+15\%$, and $+30\%$ in the Asian anthropogenic emission tracer. The mean and IAV at the surface is shown for September for the (c) 135°W and (d) 120°W slices. The error bars give the interannual variability for 2000–2011, with the lighter bars showing the max and min value, and the darker bars showing the standard deviation. The black symbols and lines represent total CO, green represents CO with the biomass-burning component removed, and blue represents CO with the North American anthropogenic component removed. The mean and IAV is shown at 500 hPa in February for (e) 30°N – 60°N , 135°W and for (f) 30°N – 60°N , 120°W , and in September for the (g) 135°W and (h) 120°W slices.

[34] We now consider when the 15% reduction in AA CO would become statistically significant in different regions of the Northern Hemisphere. Equation (1) shows that a larger number of years are needed in regions of high variability and/or where the difference between the two scenarios is small. The average Northern Hemisphere February surface concentration of CO in the standard emission scenario is shown in Figure 7a. Figure 7b shows the percent decrease in February surface CO in response to a 15% reduction in Asian anthropogenic emissions. While the concentration decreases by over 12% over the Asian source region, the decrease over the Pacific is less than 6%, and over non-Asian source regions, the percent decrease is even smaller. The interannual variability, as measured by the standard deviation (s_p) in February CO values, is shown in Figure 7c. The IAV is largest over and downwind of the anthropogenic source regions in Asia, the eastern United States, and Europe, as well as the biomass-burning region of Africa. Low variability is present over the North Pacific and tropical North Atlantic.

[35] The large response over the southern part of Asia is statistically significant with only a few years of simulation, while more years are required for statistical significance over

Russia, where the response to Asian anthropogenic emissions is smaller and IAV is higher (Figure 7d). Less than six years of each scenario are needed to achieve statistical significance over the North Pacific and parts of the western United States due to the low IAV in February in these regions, suggesting that winter observations in these locations are well suited to detecting changes in Asian anthropogenic emissions. In contrast, many decades are needed in the eastern United States, where more regional emissions are present. This experiment focuses specifically on anthropogenic emission changes over Asia, and assumes that anthropogenic emissions from other regions remain constant. If anthropogenic emissions change concurrently in other regions of the world, these changes would likely increase the number of years needed to detect the change due to Asian emissions.

[36] We next examine the number of years needed to detect a significant change due to a 15% reduction in North American anthropogenic emissions. The smaller contribution of North American emissions to the global total results in a smaller percentage response in February surface CO to the North American reduction than to the Asian reduction (Figures 7b and 7e) and requires more years to be detectable over much of the Northern Hemisphere

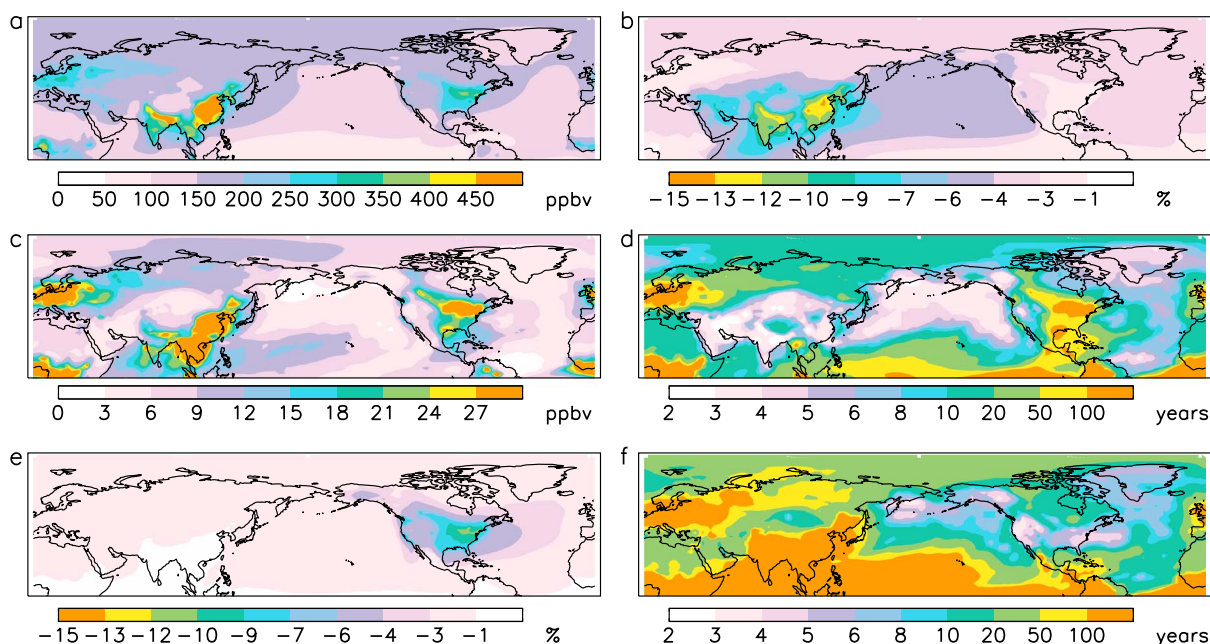


Figure 7. Maps of the surface CO over the Northern Hemisphere in February: (a) mean concentration for the standard emission case; (b) percentage reduction in CO due to a 15% reduction in Asian anthropogenic emissions; (c) the standard deviation of the February means; (d) the number of years needed to detect a significant difference between the standard and 15% Asian anthropogenic emission reduction cases; (e) the percentage reduction in CO due to a 15% reduction in North American anthropogenic emissions; (f) the number of years needed to detect a significant difference between the standard and 15% North American emission reduction cases.

(Figure 7f). However, the response to the North American reduction is still detectable with less than 6 years of each scenario over much of the United States as well as parts of the North Pacific.

[37] Unlike the February case, the large variations arising from biomass burning in September are much larger than the signal due to changes in Asian anthropogenic emissions at 135°W (Figure 6c). In the idealized case that the biomass burning contribution is perfectly known, the remaining (non-BB) CO IAV is greatly reduced, as shown by the green error bars in Figure 6c. However, the smaller relative contribution of Asian anthropogenic emissions during September still makes it difficult to separate the difference due to Asian anthropogenic emission changes from the IAV. The IAV at 120°W in September (Figure 6d) is also larger than in February. Removing the North American anthropogenic CO does little to reduce the September variability, while removing the biomass-burning CO leads to a greater reduction in variability.

[38] On a hemispheric scale, Figures 8a and 8b shows that both the background CO and the response over the Pacific to a decrease in Asian emissions is lower during September than in February, while the region of greatest extratropical variability has shifted to Siberia (Figure 8c). Consequently, we estimate that over 100 years of each scenario would be needed for statistical significance at high latitudes and over 20 years over much of the Pacific and North America (Figure 8d). However, since we know from satellite observations that 2002 and 2003 are impacted by high boreal biomass burning, these years could be excluded from an analysis focused on detecting changes in anthropogenic emissions.

Excluding these years greatly reduces the interannual variability at middle and high latitudes (Figure 8e), thus reducing the years for detection (Figure 8f).

5.2. 500 hPa Response to a Stepwise Emission Change

[39] Satellite observations provide the opportunity for trend detection over the oceans and in the free troposphere, where CO may be less affected by variability in local or regional pollution. Since both MOPITT and AIRS have high sensitivity near 500 hPa [Warner *et al.*, 2010], we examine the CO variability of the model at 500 hPa. While observation error also affects observed variability, in this step, we consider only the IAV in CO itself. In February, the IAV at 500 hPa at 135°W (Figure 6e) is larger than at the surface, and in contrast to the surface, removing the N. American anthropogenic contribution does not remove much IAV at 500 hPa for the 120°W slice (Figure 6f). The September variability, however, is smaller at 500 hPa than at the surface (Figures 6g and 6h), meaning that signals can be separated better using midtropospheric satellite observations than using surface data in this month.

[40] Considering the entire Northern Hemisphere, the geographic distribution of CO at 500 hPa (Figure 9a) in our simulation is less variable than at the surface (Figure 8a) and the influence of the Asian anthropogenic change (Figure 9b) extends further across the Pacific. While the variability at the surface is large near the Siberian biomass burning, this feature is less prominent at 500 hPa (Figure 9c). Less than 10 years of each scenario are needed to detect the 500 hPa change over much of the Pacific (Figure 9d), far less than were needed at the surface (Figure 8d).

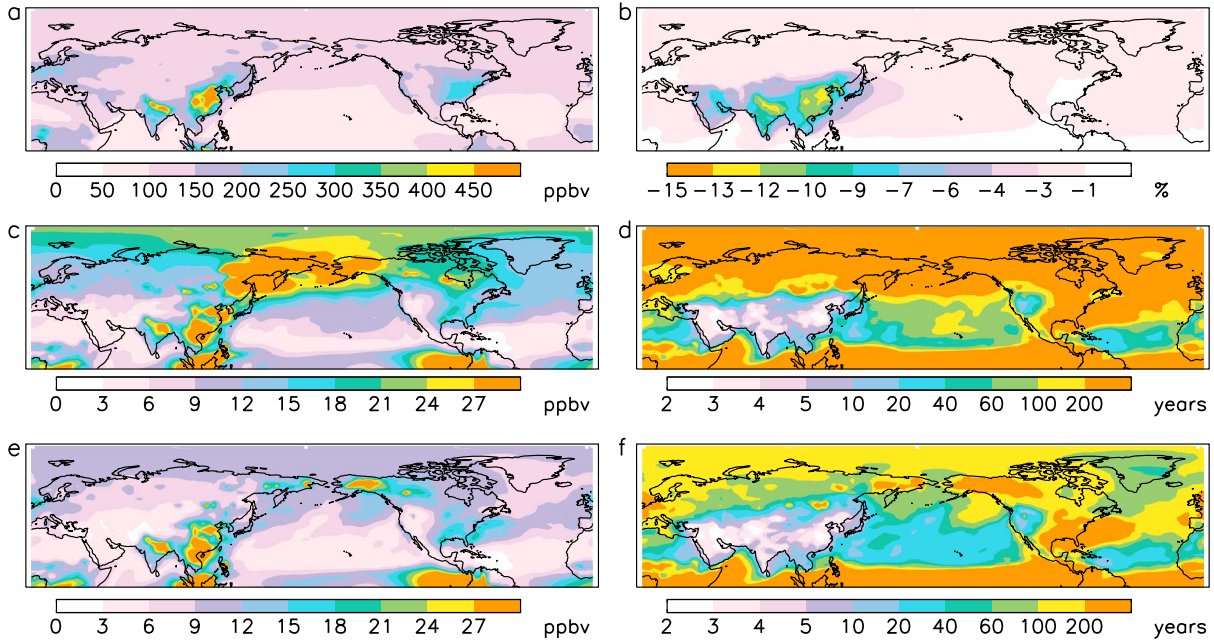


Figure 8. September surface CO: (a) multiyear mean; (b) the percent reduction in surface CO due to a 15% reduction in Asian anthropogenic emissions; (c) standard deviation; (d) number of years for the change to become statistically significant; (e) standard deviation with 2002 and 2003 removed, and (f) years for significance with 2002 and 2003 removed.

[41] The previous section showed that the model underestimates the variability seen in MOPITT. We therefore repeat the calculation for 500 hPa using the IAV in the September MOPITT data (Figure 9e) and the change in CO from the model convolved with the MOPITT kernels and a priori. MOPITT

shows greater variability than the model, and thus, the number of years for detection (Figure 9f) is also greater throughout much of the Pacific and North America than the model suggests. However, the estimate in Figure 9f suggests that detection in less than 10 years of each scenario would be possible over Asia.

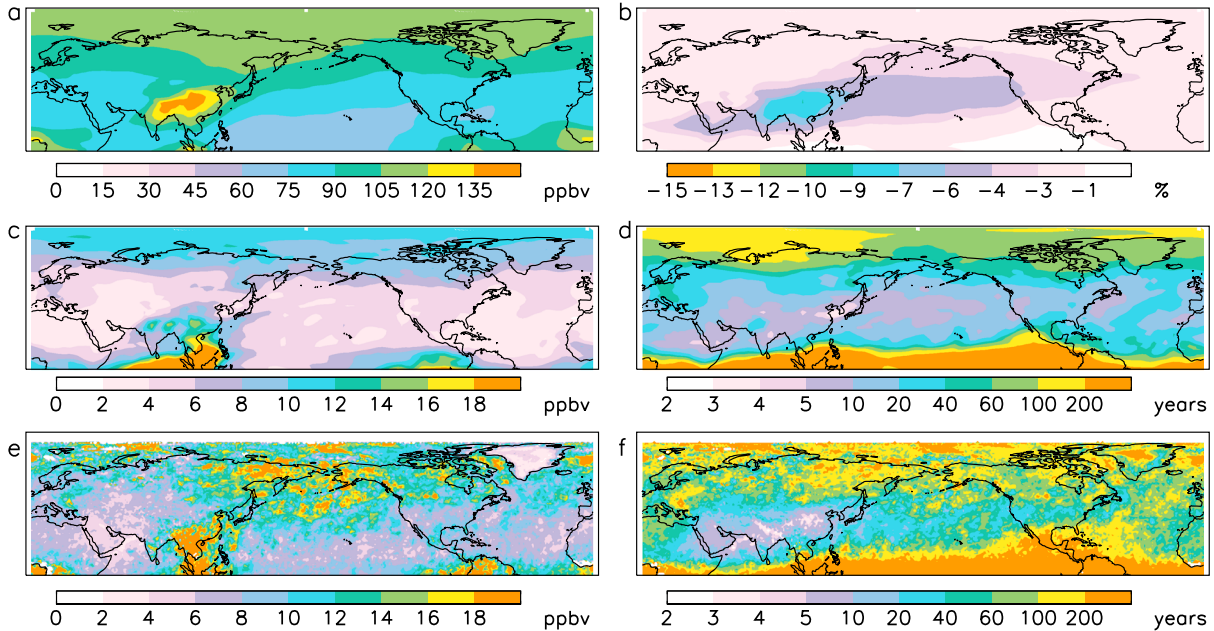


Figure 9. September 500 hPa CO: (a) multiyear model mean; (b) the percent reduction in CO concentration due to a 15% reduction in Asian anthropogenic emissions; (c) model standard deviation; (d) model-based estimate of number of years for the change to become statistically significant; (e) MOPITT standard deviation; (f) number of years for the change to become statistically significant based on the MOPITT standard deviation and the percent reduction in model CO convolved with the MOPITT kernels.

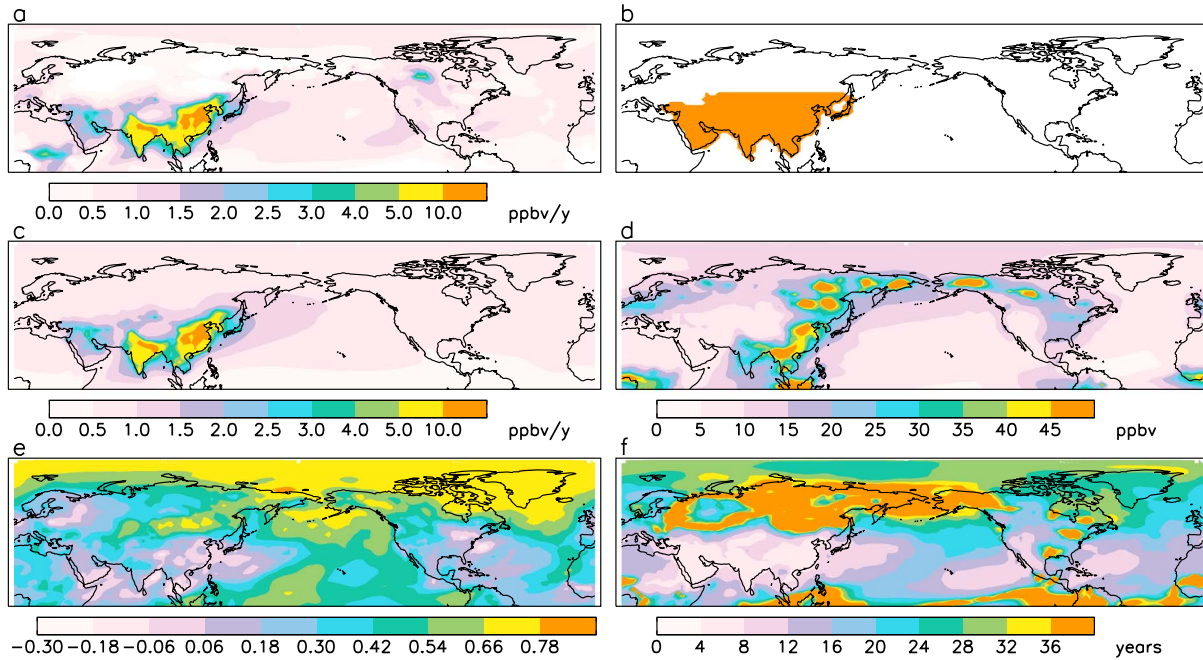


Figure 10. (a) The modeled trend in CO concentration obtained when a $3\% \text{ yr}^{-1}$ trend in anthropogenic emissions is imposed over the (b) Asian region. (c) The trend in the modeled Asian anthropogenic CO tracer for the same emission trend. The (d) standard deviation and (e) autocorrelation of the noise term in equation (4) are used to determine the (f) number of years for the trend in Figure 10a to be detectable.

5.3. Detection of a Linear Trend

[42] In the previous section, we consider the problem of detecting a step change in emissions between two sets of years, such as would result from immediate application of emission controls. However, changes in emissions often occur gradually over many years, and we are interested in detecting temporal trends due to the gradual change in emissions. This section examines the number of years needed to detect a hypothetical linear trend in Asian CO emissions. We use the same model simulation as in the previous section but impose a 3% per year increase in the Asian anthropogenic tracer for 2000–2011. We then examine the monthly mean surface CO from the model to determine when and where this imposed emission trend leads to a statistically significant trend in CO concentration.

[43] Figure 10a shows the trend in CO surface concentration when a $3\% \text{ yr}^{-1}$ increase in Asian anthropogenic emissions is applied. The Asian emission region over which the emission trend is imposed is illustrated in Figure 10b. The trend in CO surface concentration is largest over industrial regions of Asia and decreases with distance over the Pacific. The trend (ω) in Figure 10a is determined from the best fit to total CO concentration, as described in section 4. We also apply equation (3) to the model's Asian anthropogenic CO tracer to calculate the trend due specifically to changes in CO from Asian anthropogenic sources (Figure 10c). Comparison of Figure 10a with Figure 10c shows that the Asian anthropogenic trend is driving the large total trend over Asia and the smaller total trend over much of the middle and high-latitude Northern Hemisphere. However, the maxima over Africa and boreal North America, as well as the low values over the high latitudes of Europe and Asia, in Figure 10a are due to other factors such as the IAV in biomass burning.

[44] The spatial patterns of the standard deviation (σ_N) and autocorrelation (ϕ) of the noise (N) are shown in Figure 10d and 10e, respectively. The standard deviation is large over both the biomass burning regions of boreal Asia, North America, Africa, and Indonesia, and over the regions of enhanced anthropogenic emissions. In contrast, the autocorrelation is low over the anthropogenic emission regions and high over the northern latitudes. The lifetime of CO is longer at high latitudes compared to the tropics in winter [Duncan *et al.*, 2007], which could contribute to the greater autocorrelation at high latitudes.

[45] The number of years needed to detect a statistically significant trend decreases for increasing trend strength, while it increases with increasing variability and autocorrelation of the noise (equation (2)). Consequently, the smallest number of years is needed for detection (n^*) over and immediately downwind of Asia, where the change in emissions drives a large trend. Another region where n^* is small extends zonally in the 20°N – 40°N latitude band around much of the globe (Figures 10f and 11). Low variability and low autocorrelation in the noise (Figure 11) contribute to the ease of detection in this zonal band. An exception is over the eastern U.S., where the Asian anthropogenic trend does not drive the model's total CO trend (Figures 10a and 10c), and the noise has greater variability. The inland western U.S. and Hawaii stand out as regions remote from Asian emissions that may be well suited to early detection of a trend in Asian anthropogenic emissions (Figure 10e). In contrast, we predict that over 20 years are needed for detection at high latitudes, with many decades to centuries needed in biomass burning regions.

[46] Given the sensitivity of the predicted n^* to the standard deviation and autocorrelation of the modeled noise,

STRODE AND PAWSON: DETECTION OF CO TRENDS VERSUS IAV

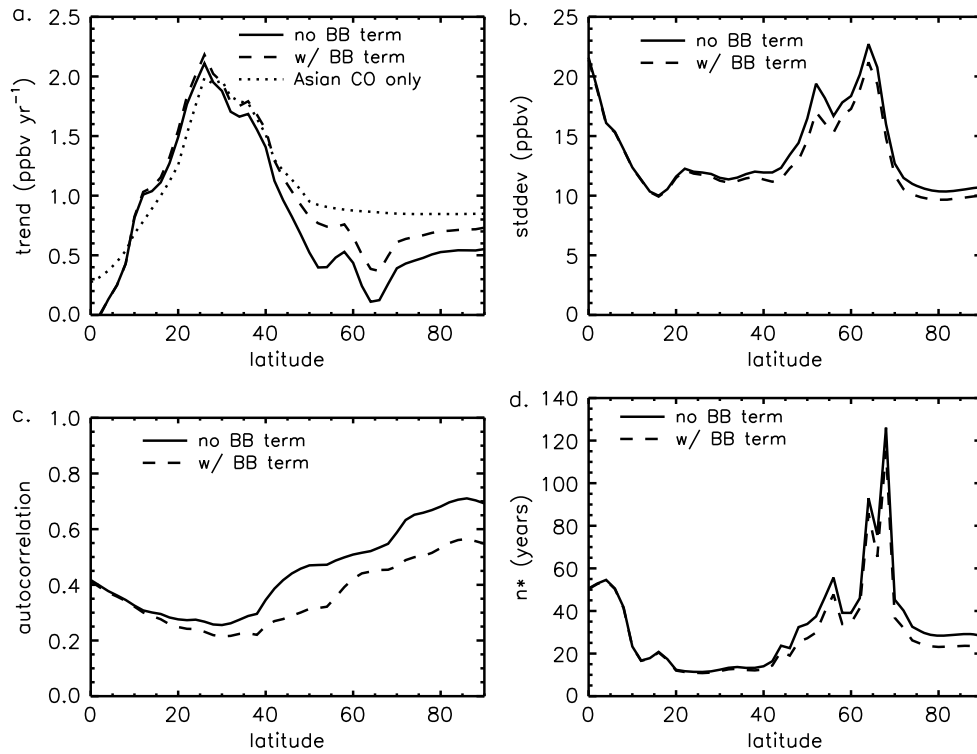


Figure 11. The (a) zonal mean of the trend, (b) standard deviation of the noise, (c) autocorrelation of the noise, and (d) the number of years for detection based on equation (2) are shown for the original regression (equation (3), solid lines) and the regression including a biomass burning term (equation (4), dashed line). The trend in the Asian anthropogenic CO tracer is shown in the dotted line on Figure 11a.

we next examine how well the modeled σ_N and ϕ agree with that of the GMD observations. The comparison of σ_N and ϕ in this section uses the discreet weekly GMD measurements of CO. We construct monthly means of the discreet GMD data and the model CO sampled on the corresponding days, as described in section 3, and calculate σ_N and ϕ for the resulting time series.

[47] Table 2 compares the values of σ_N and ϕ from the model sampled only on days with observations, the model sampled on all days, and observations at six GMD sites. Figure 5a shows the locations of these sites. The first two sites, Tae-ahn Peninsula, Korea (TAP) and Mt. Waliguan, China (WLG), are located in Asia, where a trend would likely be easy to detect. The second two sites, Wendover, Utah (UTA) and Mauna Loa, Hawaii (MLO), are remote from Asia but in regions that the model predicts would require relatively

few years for detection of a trend in Asian anthropogenic emissions. The last two sites, Shemya Island, Alaska (SHM) and Alert, Canada (ALT), are located at high latitudes, where the model predicts a larger number of years for detection. The model sampled according to the observations reproduces the observed σ_N to within 30% at five of the six stations. MLO, where the model has a larger underestimate, is a mountain station. The model may have difficulty reproducing the local meteorology, which includes upslope and downslope winds [Haas-Laursen *et al.*, 1997]. The model overestimate of σ_N at SHM is likely due to overprediction of the biomass-burning influence in some years (Figure 4b). Overall, the model tends to underestimate both σ_N and ϕ , suggesting that the predicted values of n^* are likely lower bounds. However, the model captures the higher standard deviation at the Asian sites and the higher autocorrelation at the high latitude sites seen in

Table 2. Standard Deviation (ppbv) and Autocorrelation of the Noise Term in Equation (3) for CO Observations From GMD Sites and the Simulated CO at the Corresponding Locations^a

Region	Site	Standard Deviation (N)			Autocorrelation (N)		
		Obs	Model ^b	Model monthly ^c	Obs	Model ^b	Model monthly ^c
Asia	TAP	45	41	34	-0.0022	.20	0.025
	WLG	26	20	14	0.13	-0.041	0.080
Non-Asian Region With Low n^*	UTA	10	10	7.8	0.42	0.16	0.39
	MLO	10	7.2	7.2	0.40	0.26	0.44
	SHM	10	16	15	0.60	0.50	0.66
High n^* Regions	ALT	8.6	8.5	8.8	0.79	0.72	0.76

^aThe location of the GMD sites is shown in Figure 5a.

^bModel monthly mean created by sampling the model only on days when an observation is available.

^cMonthly mean using all days in the month.

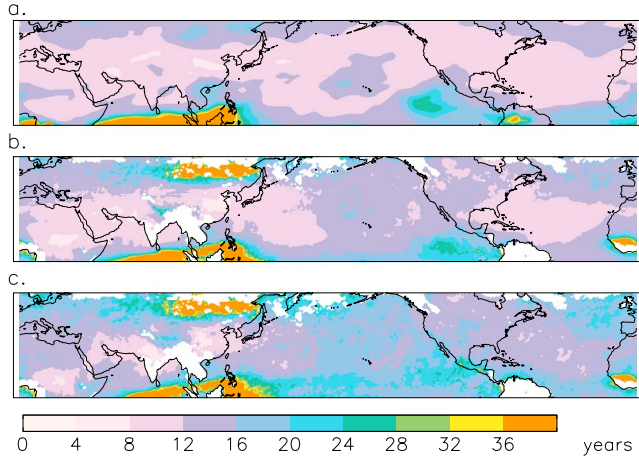


Figure 12. The number of years needed to detect a trend at 500 mb for an imposed trend in Asian anthropogenic emissions of $3\% \text{ yr}^{-1}$. The number of years is calculated from (a) the model simulation, (b) the model simulation convolved with the MOPITT averaging kernels and a priori, and (c) the simulated trend along with the σ_N and ϕ from the monthly MOPITT data for 0°N – 60°N .

the observations, evidence that the model can identify regions for rapid trend detection.

[48] *Saunio et al.* [2012] found that sampling frequency affects the IAV and trend in tropospheric ozone. *Whiteman et al.* [2011] showed that for water vapor, the fractional variability of the noise decreased as the number of sondes per month increased. Table 2 shows that sampling the model CO only on the days with a corresponding observation gives higher values of σ_N than sampling all model days within a month and is more consistent with the observed σ_N at the four sites with lower n^* predictions.

[49] IAV in boreal biomass burning contributes heavily to the need for a large number of years for anthropogenic trend detection at high latitudes. It increases the autocorrelation of the noise as well as the variability because the impact of biomass burning often extends over multiple months. The addition of the biomass burning term in equation (4) increases the magnitude of the calculated trend (Figure 11a), reducing its underestimate of the trend in the modeled Asian anthropogenic CO tracer (dotted line) north of 30° while slightly increasing the overestimate between 10°N and 30°N . The biomass burning term accounts for some of the variability that is treated as noise in equation (3). Thus, including the biomass burning term in equation (4) reduces the unexplained variability,

so the standard deviation and autocorrelation of the noise are both reduced, especially at high latitudes (Figures 11b and 11c). These factors lead to a reduction in the predicted zonal mean n^* of approximately 5–10 years north of 50°N (Figure 11d). Even larger reductions are present in particular grid boxes.

[50] We repeat the calculation of n^* for the 500 mb level to examine how quickly satellite observations of midtropospheric CO might be able to detect the imposed $3\% \text{ yr}^{-1}$ trend. The n^* calculated from the modeled CO at 500 mb (Figure 12a) is less than 12 years throughout much of the Northern Hemisphere midlatitudes, including over regions such as the eastern United States where the n^* for the surface was large (Figure 10f). Averaging the CO time series over the northeast Pacific and then using the trend and noise of the regionally averaged CO yields an n^* value of 12 years for the region from 30°N – 60°N , 179.5°W – 135°W . Following the approach of *Weatherhead et al.* [1998] to account for the uncertainty in n^* resulting from uncertainty in our estimated autocorrelation, we find a 95% confidence interval of 9–15 years on the northeast Pacific n^* (Table 3).

[51] The calculation of n^* from simulated CO incorporates effects of biomass burning and transport on CO variability but does not account for all the sources of variability. Furthermore, there is significant variability in the MOPITT CO averaging kernels [*Deeter et al.*, 2003]. Application of the kernel and a priori to an in situ profile reduces how much vertical structure is resolved [*Emmons et al.*, 2007]. CO concentrations and their variability differ by altitude (Figure 1), so the variability in the 500 hPa retrieval could be impacted by variability at other levels. Figure 12b shows the n^* values that result from convolving the modeled CO, including the imposed emission trend, with the monthly MOPITT averaging kernels and a priori. Compared to the purely model-based calculation, the application of the kernel increases n^* over much of the northeast Pacific and leads to large n^* values over Siberia, a region where MOPITT has low degrees of freedom in winter and where biomass burning induces large IAV in lower tropospheric CO. Table 3 quantifies the impact of applying the kernels and a priori to the simulated CO over the northeast Pacific. The increase in σ_N leads to a 3 year increase in n^* , but this increase is small relative to the confidence interval.

[52] We next examine how using observed rather than modeled noise will affect our calculation. We apply equation (3) to the monthly level 3 MOPITT 500 mb CO retrievals for 2000–2011 and use the resulting noise to calculate σ_N and ϕ . We use this σ_N and ϕ along with the trend calculated from the modeled CO convolved with the MOPITT kernels to

Table 3. Standard Deviation (ppbv) and Autocorrelation of the Noise Term in Equation (3), as Well as the Resulting n^* , for CO at 500 mb Averaged Over the Northeast Pacific (30°N – 60°N , 179.5°W – 135°W)^a

	Standard Deviation (N)	Autocorrelation (N)	Years for Detection (95% Confidence Interval)
Simulation	5.3	0.66	12 (9–15)
Simulation Convolved With MOPITT	7.6	0.65	15 (11–19)
MOPITT	10	0.64	18 ^b (14–23)
Simulation at North Pacific GMD Sites	11	0.43	20 (17–24)
North Pacific GMD	14	0.36	22 ^c (19–26)

^aThe same quantities are also given for the North Pacific GMD sites shown in Figures 2–4 and the model sampled at those sites.

^bCalculated using the trend from the simulation convolved with MOPITT.

^cCalculated using the average trend from the simulation sampled at the GMD sites.

calculate the n^* values shown in Figure 12c. Figure 12c shows that using the noise from the MOPITT retrievals rather than from the model further increases n^* over much of the Northern Hemisphere. However, regions of low n^* are still present, indicating that a decade-long record of satellite observations of midtropospheric CO has potential for detecting future trends of this magnitude. Using the observed noise for the North Pacific average increases σ_N substantially but has little impact on ϕ . n^* increases to 18 years, a 50% increase over the value calculated from the model alone (Table 3).

[53] Table 3 also shows the same calculation for the average of the model trend, ϕ and σ , sampled at the location of the six GMD sites shown in Figures 2–4, and for the model trend combined with the ϕ and σ calculated from the GMD data. Although the model underestimates the observed σ , it overestimates the observed ϕ , leading to a similar value of n^* (20 years) to that predicted by the observations (22 years). These values are slightly larger than the MOPITT-based estimate of 18 years, but the confidence intervals overlap.

6. Conclusions

[54] Separating the effect of changing anthropogenic emissions from natural variability in transport and biomass burning is important for detecting trends against a backdrop of IAV. The competing effects of economic growth and increased control technology are likely to alter anthropogenic CO emissions in the future, impacting air quality and methane lifetime. The strength and direction of future trends in CO emissions is still uncertain, and satellite and surface observations can help constrain how emissions are changing over time. However, year-to-year differences in biomass burning make a large contribution to the IAV of CO, complicating the process of attributing anthropogenic changes in a short time series. This study uses model simulations to estimate the number of years of observations needed to detect significant trends due to specified changes in CO emissions from Asia and to identify regions well suited to detecting changes quickly.

[55] The model interannual variability is well correlated with that seen in September data at GMD sites in the North Pacific, due to its ability to capture interannual variation in the boreal biomass burning influence. The modeled interannual variability in the CO column over the north Pacific is well correlated with MOPITT ($r^2 > 0.6$) in both February and September, but the model underestimates the standard deviation. Consequently, our model-based estimates of the years to detect a change in Asian anthropogenic emissions are likely a lower bound.

[56] We find that at 135°W in the North Pacific, upwind of the west coast of the North America, the February CO concentration change due to an Asian anthropogenic emission change of 30% exceeds the interannual variability of the model at the surface. The lower biomass burning emissions during February make this month ideal for detecting anthropogenic effects on CO inflow to North America. In contrast, the IAV in September exceeds the effect of even a large change in anthropogenic emissions. However, satellite observations of midtropospheric CO over the North Pacific could be useful for detecting anthropogenic changes in September, since the interannual variability is lower and the influence of Asian emission reductions extends further at 500 hPa than at the surface.

[57] We apply the method of *Weatherhead et al.* [1998] to our simulated CO to estimate the number of years needed to detect a trend in monthly surface CO resulting from a 3% per year in Asian anthropogenic CO emissions. We find that an emission trend of this magnitude could lead to a significant trend in surface CO in less than 12 years in the southwestern United States.

[58] The estimate above assumes that local emissions remain constant; if local emissions change in the opposite direction as Asian emissions, that effect could diminish or cancel the impact of the changing Asian CO contribution. Furthermore, the 12 year simulation and the MOPITT record used to estimate variability in this study are not long enough to capture variability on decadal and longer timescales and may thus underestimate the timescales for detection. The model underestimate of the observed variability also makes the model-based estimates of detection time lower limits.

[59] We apply the same method to the model CO at 500 mb and find that the trend is significant in less than 12 years throughout much of the northern midlatitudes. However, the MOPITT 500 mb retrievals include greater unexplained variability than the model CO. Including this variability as well as applying the MOPITT averaging kernels to the modeled trend increases the predicted number of years needed to detect a statistically significant trend over the northeast Pacific from 12 to 18. The predicted number of years remains small over Asia and the northwest Pacific, however, highlighting the value of satellite observations over source regions. *Worden et al.* [2013] showed the importance of satellite records longer than a decade for trend detection, and pointed out the possibility of a 20 year record with the inclusion of future IASI instruments. Our results suggest that detection of trends in Asian anthropogenic emissions would be possible on this timescale.

[60] Overall, the results show that a model-based analysis of observed CO concentrations can be used to isolate potential trends in emissions and the timescales for detecting them. For instance, regional CO variations arising from biomass-burning emissions at remote locations can be separated from the other contributions, as long as sufficient observations are available to characterize emissions of CO by biomass burning, as is done by the GFED emissions databases used in this study. This capability could be especially useful if the magnitude or variability biomass burning emissions changes in the future.

[61] Both surface-based and space-based observations of CO are useful for detecting anthropogenic emissions trends in remote locations, with the different data sets being most useful in different locations. The specific application to downstream detection of Asian Anthropogenic CO trends examined in this study can be adapted to detecting emission trends from different regions and, most likely, for different constituents, such as carbon dioxide.

[62] **Acknowledgments.** This research was supported by NASA, including substantial computing resources provided by the High-Performance Computing Program. We thank Eric Nielsen and Lesley Ott for assistance with the model. We thank Paul Novelli for useful discussions on the GMD data and Merritt Deeter for helpful discussions of the MOPITT data.

References

- Allen, D. J., P. Kasibhatla, A. M. Thompson, R. B. Rood, B. G. Doddridge, K. E. Pickering, R. D. Hudson, and S.-J. Lin (1996), Transport-induced interannual variability of carbon monoxide determined using a chemistry and transport model, *J. Geophys. Res.*, *101*, 28,655–28,669.

- Allen, D., K. Pickering, and M. Fox-Rabinovitz (2004), Evaluation of pollutant outflow and CO sources during TRACE-P using model-calculated, aircraft-based, and Measurements of Pollution in the Troposphere (MOPITT)-derived CO concentrations, *J. Geophys. Res.*, *109*, D15S03, doi:10.1029/2003JD004250.
- Aumann, H. H., et al. (2003), AIRS/AMSU/HSB on the Aqua Mission: Design, science objectives, data products, and processing systems, *IEEE Trans. Geosci. Remote Sens.*, *41*, 253–264.
- Bey, I., D. J. Jacob, J. A. Logan, and R. M. Yantosca (2001), Asian chemical outflow to the Pacific: Origins, pathways and budgets, *J. Geophys. Res.*, *106*, 23,097–23,113.
- Clerbaux, C., et al. (2009), Monitoring of atmospheric composition using the thermal infrared IASI/MetOp sounder, *Atmos. Chem. Phys.*, *9*(16), 6041–6054.
- Crutzen, P. (1973), A discussion of the chemistry of some minor constituents in the stratosphere and troposphere, *Pure App. Geophys.*, *106*, 1385–1399.
- Deeter, M. N., et al. (2003), Operational carbon monoxide retrieval algorithm and selected results for the MOPITT instrument, *J. Geophys. Res.*, *108*(D14), 4399, doi:10.1029/2002JD003186.
- Deeter, M. N., L. K. Emmons, D. P. Edwards, J. C. Gille, and J. R. Drummond (2004), Vertical resolution and information content of CO profiles retrieved by MOPITT, *Geophys. Res. Lett.*, *31*, L15112, doi:10.1029/2004GL020235.
- Deeter, M. N., et al. (2010), The MOPITT version 4 CO product: Algorithm enhancements, validation, and long-term stability, *J. Geophys. Res.*, *115*, D07306, doi:10.1029/2009JD013005.
- Duncan, B. N., and J. A. Logan (2008), Model analysis of the factors regulating the trends and variability of carbon monoxide between 1988 and 1997, *Atmos. Chem. Phys.*, *8*, 7389–7403.
- Duncan, B. N., J. A. Logan, I. Bey, I. A. Megretskaya, R. M. Yantosca, P. C. Novelli, N. B. Jones, and C. P. Rinsland (2007), Global budget of CO, 1988–1997: Source estimates and validation with a global model, *J. Geophys. Res.*, *112*, D22301, doi:10.1029/2007JD008459.
- Edwards, D. P., et al. (2004), Observations of carbon monoxide and aerosols from the Terra satellite: Northern Hemisphere variability, *J. Geophys. Res.*, *109*, D24202, doi:10.1029/2004JD004727.
- Edwards, D. P., G. Pétron, P. C. Novelli, L. K. Emmons, J. C. Gille, and J. R. Drummond (2006), Southern Hemisphere carbon monoxide interannual variability observed by Terra/Measurement of Pollution in the Troposphere (MOPITT), *J. Geophys. Res.*, *111*, D16303, doi:10.1029/2006JD007079.
- Emmons, L. K., et al. (2004), Validation of Measurements of Pollution in the Troposphere (MOPITT) CO retrievals with aircraft in situ profiles, *J. Geophys. Res.*, *109*, D03309, doi:10.1029/2003JD004101.
- Emmons, L. K., G. G. Pfister, D. P. Edwards, J. C. Gille, G. Sachse, D. Blake, S. Wofsy, C. Gerbig, D. Matross, and P. Nédélec (2007), Measurements of Pollution in the Troposphere (MOPITT) validation exercises during summer 2004 field campaigns over North America, *J. Geophys. Res.*, *112*, D12S02, doi:10.1029/2006JD007833.
- Emmons, L. K., D. P. Edwards, M. N. Deeter, J. C. Gille, T. Campos, P. Nédélec, P. Novelli, and G. Sachse (2009), Measurements of Pollution in The Troposphere (MOPITT) validation through 2006, *Atmos. Chem. Phys.*, *9*(5), 1795–1803, doi:10.5194/acp-9-1795-2009.
- George, M., et al. (2009), Carbon monoxide distributions from the IASI/METOP mission: Evaluation with other space-borne remote sensors, *Atmos. Chem. Phys.*, *9*(21), 8317–8330, doi:10.5194/acp-9-8317-2009.
- Granier, C., et al. (2011), Evolution of anthropogenic and biomass burning emissions of air pollutants at global and regional scales during the 1980–2010 period (2011), *Clim. Change*, *109*(1–2), 163–190, doi:10.1007/s10584-011-0154-1.
- Haas-Laursen, D. E., D. E. Hartley, and T. J. Conway (1997), Consistent sampling methods for comparing models to CO₂ flask data, *J. Geophys. Res.*, *102*(D15), 19,059–19,071.
- Heald, C. L., et al. (2003), Asian outflow and trans-Pacific transport of carbon monoxide and ozone pollution: An integrated satellite, aircraft, and model perspective, *J. Geophys. Res.*, *108*, 4804, doi:10.1029/2003JD003507, D24.
- Hsu, N. C., C. Li, N. A. Krotkov, Q. Liang, K. Yang, and S.-C. Tsay (2012), Rapid transpacific transport in autumn observed by the A-train satellites, *J. Geophys. Res.*, *117*, D06312, doi:10.1029/2011JD016626.
- Jaffe, D., A. Mahura, J. Kelley, J. Atkins, P. C. Novelli, and J. Merrill (1997), Impact of Asian emissions on the remote North Pacific atmosphere: Interpretation of CO data from Shemya, Guam, Midway and Mauna Loa, *J. Geophys. Res.*, *102*(D23), 28,627–28,635, doi:10.1029/96JD02750.
- Jaffe, D., I. Bertsch, L. Jaeglé, P. Novelli, J. S. Reid, H. Tanimoto, R. Vingarzan, and D. L. Westphal (2004), Long-range transport of Siberian biomass burning emissions and impact on surface ozone in western North America, *Geophys. Res. Lett.*, *31*, L16106, doi:10.1029/2004GL020093.
- Kasischke, E. S., E. J. Hyer, P. C. Novelli, L. P. Bruhwiler, N. H. F. French, A. I. Sukhinin, J. H. Hewson, and B. J. Stocks (2005), Influences of boreal fire emissions on Northern Hemisphere atmospheric carbon and carbon monoxide, *Global Biogeochem. Cycles*, *19*, GB1012, doi:10.1029/2004GB002300.
- Khalil, M. A. K., and R. A. Rasmussen (1988), Carbon monoxide in the Earth's atmosphere: Indications of a global increase, *Nature*, *332*, 242–245.
- Khalil, M. A. K., and R. A. Rasmussen (1994), Global decrease in atmospheric carbon monoxide concentration, *Nature*, *370*, 639–641.
- Kopacz, M., et al. (2010), Global estimates of CO sources with high resolution by adjoint inversion of multiple satellite datasets (MOPITT, AIRS, SCIAMACHY, TES), *Atmos. Chem. Phys.*, *10*, 855–876, doi:10.5194/acp-10-855-2010.
- Lamarque, J.-F., et al. (2010), Historical (1850–2000) gridded anthropogenic and biomass burning emissions of reactive gases and aerosols: Methodology and application, *Atmos. Chem. Phys.*, *10*, 7017–7039, doi:10.5194/acp-10-7017-2010.
- Langenfelds, R. L., R. J. Francey, B. C. Pak, L. P. Steele, J. Lloyd, C. M. Trudinger, and C. E. Allison (2002), Interannual growth rate variations of atmospheric CO₂ and its δ¹³C, H₂, CH₄, and CO between 1992 and 1999 linked to biomass burning, *Global Biogeochem. Cycles*, *16*(3), 1048, doi:10.1029/2001GB001466.
- Liang, Q., L. Jaeglé, D. A. Jaffe, P. Weiss-Penzias, A. Heckman, and J. A. Snow (2004), Long-range transport of Asian pollution to the northeast Pacific: Seasonal variations and transport pathways of carbon monoxide, *J. Geophys. Res.*, *109*, D23S07, doi:10.1029/2003JD004402.
- Liang, Q., L. Jaeglé, and J. M. Wallace (2005), Meteorological indices for Asian outflow and transpacific transport on daily to interannual timescales, *J. Geophys. Res.*, *110*, D18308, doi:10.1029/2005JD005788.
- Lin, S.-J. (2004), A vertically Lagrangian finite-volume dynamical core for global models, *Mon. Weather Rev.*, *132*, 2293–2307.
- Liu, H., D. J. Jacob, I. Bey, R. M. Yantosca, B. N. Duncan, and G. W. Sachse (2003), Transport pathways for Asian pollution outflow over the Pacific: Interannual and seasonal variations, *J. Geophys. Res.*, *108*(D20), 8786, doi:10.1029/2002JD003102.
- Logan, J. A., M. J. Prather, S. C. Wofsy, and M. B. McElroy (1981), Tropospheric chemistry: A global perspective, *J. Geophys. Res.*, *86*(C8), 7210–7254.
- Logan, J. A., I. Megretskaya, R. Nassar, L. T. Murray, L. Zhang, K. W. Bowman, H. M. Worden, and M. Luo (2008), Effects of the 2006 El Niño on tropospheric composition as revealed by data from the Tropospheric Emission Spectrometer (TES), *Geophys. Res. Lett.*, *35*, L03816, doi:10.1029/2007GL031698.
- Macdonald, A. M., K. G. Anlauf, W. R. Leitch, E. Chan, and D. W. Tarasick (2011), Interannual variability of ozone and carbon monoxide at the Whistler high elevation site: 2002–2006, *Atmos. Chem. Phys.*, *11*, 11,431–11,446, doi:10.5194/acp-11-11431-2011.
- McMillan, W. W., C. Barnet, L. Strow, M. T. Chahine, M. L. McCourt, J. X. Warner, P. C. Novelli, S. Korontzi, E. S. Maddy, and S. Datta (2005), Daily global maps of carbon monoxide from NASA's Atmospheric Infrared Sounder, *Geophys. Res. Lett.*, *32*, L11801, doi:10.1029/2004GL021821.
- McMillan, W. W., et al. (2008), AIRS views transport from 12 to 22 July 2004 Alaskan/Canadian fires: Correlation of AIRS CO and MODIS AOD with forward trajectories and comparison of AIRS CO retrievals with DC-8 in situ measurements during INTEX-A/ICARTT, *J. Geophys. Res.*, *113*, D20301, doi:10.1029/2007JD009711.
- McMillan, W. W., K. D. Evans, C. D. Barnet, E. S. Maddy, G. W. Sachse, and G. S. Diskin (2011), Validating the AIRS version 5 CO retrieval with DACOM in situ measurements during INTEX-A and -B, *IEEE Trans. Geosci. Remote Sens.*, *49*(7), 2802–2813.
- Mu, M., et al. (2011), Daily and 3-hourly variability in global fire emissions and consequences for atmospheric model predictions of carbon monoxide, *J. Geophys. Res.*, *116*, D24303, doi:10.1029/2011JD016245.
- Naik, V., et al. (2013), Preindustrial to present-day changes in tropospheric hydroxyl radical and methane lifetime from the Atmospheric Chemistry and Climate Model Intercomparison Project (ACCMIP), *Atmos. Chem. Phys.*, *13*, 5277–5298, doi:10.5194/acp-13-5277-2013.
- Novelli, P. C., and K. A. Masarie (2010), Atmospheric carbon monoxide dry air mole fractions from the NOAA ESRL Carbon Cycle Cooperative Global Air Sampling Network, 1988–2009, Version: 2010-07-14, Path: ftp://ftp.cmdl.noaa.gov/ccg/co/flask/event/.
- Novelli, P. C., K. A. Masarie, P. M. Lang, B. D. Hall, R. C. Myers, and J. W. Elkins (2003), Reanalysis of tropospheric CO trends: Effects of the 1997–1998 wildfires, *J. Geophys. Res.*, *108*(D15), 4464, doi:10.1029/2002JD003031.
- Ohara, T., H. Akimoto, J. Kurokawa, N. Horii, K. Yamaji, X. Yan, and T. Hayasaka (2007), An Asian emission inventory of anthropogenic emission sources for the period 1980–2020, *Atmos. Chem. Phys.*, *7*, 4419–4444.
- Ott, L., B. Duncan, S. Pawson, P. Colarco, M. Chin, C. Randles, T. Diehl, and E. Nielsen (2010), Influence of the 2006 Indonesian biomass burning aerosols on tropical dynamics studied with the GEOS5 AGCM, *J. Geophys. Res.*, *115*, D14121, doi:10.1029/2009JD013181.
- Pfister, G. G., L. K. Emmons, D. P. Edwards, A. Arellano, G. Sachse, and T. Campos (2010), Variability of springtime transpacific pollution transport during 2000–2006: The INTEX-B mission in the context of previous years, *Atmos. Chem. Phys.*, *10*, 1345–1359.

- Pfister, G. G., J. Avise, C. Wiedinmyer, D. P. Edwards, L. K. Emmons, G. D. Diskin, J. Podolske, and A. Wisthaler (2011a), CO source contribution analysis for California during ARCTAS-CARB, *Atmos. Chem. Phys.*, *11*(15), 7515–7532, doi:10.5194/acp-11-7515-2011.
- Pfister, G. G., et al. (2011b), Characterizing summertime chemical boundary conditions for air masses entering the US West Coast, *Chem. Phys.*, *11*(4), 1769–1790, doi:10.5194/acp-11-1769-2011.
- Rienecker, M. M., et al. (2008), The GEOS-5 Data Assimilation System—Documentation of Versions 5.0.1, 5.1.0, and 5.2.0., Technical Report Series on Global Modeling and Data Assimilation, 27.
- Rienecker, M. M., et al. (2011), MERRA-NASA's modern-era retrospective analysis for research and applications, *J. Clim.*, *24*(14), 3624–3648, doi:10.1175/JCLI-D-11-00015.1.
- Rinsland, C. P., et al. (2006), Nadir measurements of carbon monoxide distributions by the Tropospheric Emission Spectrometer instrument onboard the Aura Spacecraft: Overview of analysis approach and examples of initial results, *Geophys. Res. Lett.*, *33*, L22806, doi:10.1029/2006GL027000.
- Saunio, M., L. Emmons, J.-F. Lamarque, S. Tilmes, C. Wespes, V. Thouret, and M. Schulze (2012), Impact of sampling frequency in the analysis of tropospheric ozone observations, *Atmos. Chem. Phys.*, *12*, 6757–6773, doi:10.5194/acp-12-6757-2012.
- Shindell, D. T., et al. (2006), Multimodel simulations of carbon monoxide: Comparison with observations and projected near-future changes, *J. Geophys. Res.*, *111*, D19306, doi:10.1029/2006JD007100.
- Stohl, A. (2001), A 1-year Lagrangian climatology of airstreams in the Northern Hemisphere troposphere and lowermost stratosphere, *J. Geophys. Res.*, *106*, 7263–7279.
- Stohl, A., S. Eckhardt, C. Forster, P. James, and N. Spichtinger (2002), On the pathways and timescales of intercontinental air pollution transport, *J. Geophys. Res.*, *107*(D23), 4684, doi:10.1029/2001JD001396.
- Szopa, S., D. A. Hauglustaine, and P. Ciais (2007), Relative contributions of biomass burning emissions and atmospheric transport to carbon monoxide interannual variability, *Geophys. Res. Lett.*, *34*, L18810, doi:10.1029/2007GL030231.
- Taschetto, A. S., and M. H. England (2008), Estimating ensemble size requirements of AGCM simulations, *Meteorol. Atmos. Phys.*, *100*, 23–36.
- Thompson, A. M. (1992), The oxidizing capacity of the Earth's atmosphere: Probable past and future changes, *Science*, *256*, 1157–1165.
- Thoning, K. W., P. P. Tans, and W. D. Komhyr (1989), Atmospheric carbon dioxide at Mauna Loa, 2, Analysis of the NOAA GMCC data 1974–1985, *J. Geophys. Res.*, *94*, 8549–8576.
- Tiao, G. C., G. C. Reinsel, D. Xu, J. H. Pedrick, X. Zhu, A. J. Miller, J. J. DeLuisi, C. L. Mateer, and D. J. Wuebbles (1990), Effects of autocorrelation and temporal sampling schemes on estimates of trend and spatial correlation, *J. Geophys. Res.*, *95*, 20,507–20,517.
- Turquety, S., et al. (2008), CO emission and export from Asia: An analysis combining complementary satellite measurements (MOPITT, SCIAMACHY and ACE-FTS) with global modeling, *Atmos. Chem. Phys.*, *8*(17), 5187–5204, doi:10.5194/acp-8-5187-2008.
- U.S. Environmental Protection Agency (2008), Latest Findings on Air Quality-Status and Trends through 2006, EPA-454/R-07-007. [Available at: <http://www.epa.gov/air/airtrends/2007/>.]
- Val Martin, M., J. A. Logan, R. A. Kahn, F.-Y. Leung, D. L. Nelson, and D. J. Diner (2010), Smoke injection heights from fires in North America: Analysis of 5 years of satellite observations, *Atmos. Chem. Phys.*, *10*, 1491–1510.
- Van der Werf, G. R., J. T. Randerson, L. Giglio, G. J. Collatz, P. S. Kasibhatla, and A. F. Arellano Jr. (2006), Interannual variability in global biomass burning emissions from 1997 to 2004, *Atmos. Chem. Phys.*, *6*, 3423–3441.
- Van der Werf, G. R., J. T. Randerson, L. Giglio, G. J. Collatz, M. Mu, P. S. Kasibhatla, D. C. Morton, R. S. DeFries, Y. Jin, and T. T. van Leeuwen (2010), Global fire emissions and the contribution of deforestation, savanna, forest, agricultural, and peat fires (1997–2009), *Atmos. Chem. Phys.*, *10*, 11,707–11,735, doi:10.5194/acp-10-11707-2010.
- Van Vuuren, D. P., et al. (2011), The representative concentration pathways: An overview, *Clim. Change*, *109*, 5–31, doi:10.1007/s10584-011-0148-z.
- von Storch, H., and F. W. Zwiers (1999), *Statistical Analysis in Climate Research*, Cambridge Univ. Press, New York.
- Voulgarakis, A., N. H. Savage, O. Wild, P. Braesicke, P. J. Young, G. D. Carver, and J. A. Pyle (2010), Interannual variability of tropospheric composition: The influence of changes in emissions, meteorology and clouds, *Atmos. Chem. Phys.*, *10*, 2491–2506.
- Warner, J. X., M. M. Comer, C. D. Barnet, W. W. McMillan, W. Wolf, E. Maddy, and G. Sachse (2007), A comparison of satellite tropospheric carbon monoxide measurements from AIRS and MOPITT during INTEX-A, *J. Geophys. Res.*, *112*, D12S17, doi:10.1029/2006JD007925.
- Warner, J. X., Z. Wei, L. L. Strow, C. D. Barnet, L. C. Sparling, G. Diskin, and G. Sachse (2010), Improved agreement of AIRS tropospheric carbon monoxide products with other EOS sensors using optimal estimation retrievals, *Atmos. Chem. Phys.*, *10*, 9521–9533.
- Weatherhead, E. C., et al. (1998), Factors affecting the detection of trends: Statistical considerations and applications to environmental data, *J. Geophys. Res.*, *103*(D14), 17,149–17,161.
- Weatherhead, E. C., A. J. Stervermer, and B. E. Schwartz (2002), Detecting environmental changes and trends, *Phys. Chem. Earth*, *27*, 399–403.
- Whiteman, D. N., K. C. Vermeesch, L. D. Oman, and E. C. Weatherhead (2011), The relative importance of random error and observation frequency in detecting trends in upper tropospheric water vapor, *J. Geophys. Res.*, *116*, D21118, doi:10.1029/2011JD016610.
- Worden, H. M., et al. (2013), Decadal record of satellite carbon monoxide observations, *Atmos. Chem. Phys.*, *13*(2), 837–850.
- Wotawa, G., P. C. Novelli, M. Trainer, and C. Granier (2001), Inter-annual variability of summertime CO concentrations in the Northern Hemisphere explained by boreal forest fires in North America and Russia, *Geophys. Res. Lett.*, *28*(24), 4575–4578.
- Yashiro, H., S. Sugawara, K. Sudo, S. Aoki, and T. Nakazawa (2009), Temporal and spatial variations of carbon monoxide over the western part of the Pacific Ocean, *J. Geophys. Res.*, *114*, D08305, doi:10.1029/2008JD010876.
- Yienger, J. J., M. Galanter, T. A. Holloway, M. J. Phadnis, S. K. Guttikunda, C. R. Carmichael, W. J. Moxim, and H. Levy II (2000), The episodic nature of air pollution transport from Asia to North America, *J. Geophys. Res.*, *105*, 26,931–26,945.
- Yurganov, L., W. McMillan, A. Dzhola, E. Grechko, N. Jones, and G. van der Werf (2008), Global AIRS and MOPITT CO measurements: Validation, comparison, and links to biomass burning variations and carbon cycle, *J. Geophys. Res.*, *113*, D09301, doi:10.1029/2007JD009229.